Dynamical magnetic skyrmions

Y. Zhou,[1,2] E. Iacocca,[3] A. Awad,[3] R. K. Dumas,[3] F. C. Zhang,[4,1] H. B. Braun,[5,6] and J. Åkerman[3,7]

[1]*Department of Physics, The University of Hong Kong, Hong Kong, P. R. China*
[2]*Center of Theoretical and Computational Physics, Univ. of Hong Kong, P. R. China*
[3]*Physics Department, University of Gothenburg, 412 96, Gothenburg, Sweden*
[4]*Department of Physics, Zhejiang University, Hang Zhou, P. R. China*
[5]*UCD School of Physics, University College Dublin, Dublin 4, Ireland*
[6]*Theoretical Physics and Department of Materials, ETH Zürich, CH-8093 Zürich, Switzerland*
[7]*Material Physics, School of ICT, Royal Institute of Technology, Electrum 229, 164 40, Kista, Sweden*

arXiv:1404.3281v2 [cond-mat.mes-hall] 18 Sep 2014

Spin transfer torque (STT) affords magnetic nanodevices the potential to act as memory, computing, and microwave elements operating at ultra-low currents and at a low energy cost. Spin transfer torque is not only effective in manipulating well-known magnetic structures, such as domain walls and vortices, but can also nucleate previously unattainable nano-magnetic objects, such as magnetic droplets and skyrmions. While the droplet and the skyrmion are both solitons, the former is inherently dynamic and non-topological, whereas the latter is static but topologically protected. Here we show that it is possible to combine these properties into a novel topologically protected *dynamical skyrmion*, which adds additional degrees of freedom, and functionality, to both droplet and skyrmion based applications. Unlike static skyrmions, the dynamical skyrmion can be nucleated and sustained *without* Dzyaloshinskii-Moriya interaction (DMI) or dipole-dipole interaction (DDI), and is a generic soliton solution independent of STT and damping once nucleated. In the presence of large DMI, the dynamical skyrmion experiences strong breathing with particular promise for skyrmion-based memory and microwave applications.

There has been a recent rapid increase in the research of magnetic skyrmions [1–9], which are particle-like topological solitons originally discovered in bulk ferromagnets lacking inversion symmetry, such as the non-centrosymmetric MnSi and FeCoSi [10, 11] and later also in thin films of similar materials [11, 12]. The magnetic skyrmion's spin texture results from a balance between the ordinary ferromagnetic exchange coupling, the Dzyaloshinskii-Moriya interaction (DMI), and the Zeeman energy from the applied field. Very recently, skyrmions were also proposed as the next generation magnetic information carriers in ultrathin magnetic nanowires where asymmetric interfaces provide the necessary DMI [13–15]. As information carriers, it is vital to nucleate isolated skyrmions in opposition to the skyrmion lattice phase observed for non-centrosymmetric thin films [12]. Such isolated skyrmions were recently demonstrated experimentally by using spin-polarized tunneling microscopy (STM) at zero field in one monolayer of Fe grown in Ir(111) [16].

In parallel with this rapid development, a novel dynamic, dissipative, and non-topological magnetic soliton, the so-called magnetic droplet [17], was very recently experimentally demonstrated [18] using spin transfer torque (STT) in nano-contact spin torque oscillators (NC-STOs) with perpendicular magnetic anisotropy (PMA) free layers. While originally considered a theoretical curiosity, only stable in magnetic PMA films with zero spin wave damping [19, 20], the advent of STT [21, 22] made it possible to locally create an effectively loss-less spin wave medium [23, 24] with the required material properties for droplet nucleation, control, and manipulation [17, 25].

While droplets and skyrmions have up to this point been studied entirely separately, with little cross-fertilization between the two, they are in fact strongly related. The fundamental properties that so far separate them are their dynamical, topological, and dissipative character. The droplet is dynamic in the sense that all its spins precess at a single frequency; in a skyrmion the spin texture stays static and only its spatial extent can be varied by external factors e.g. ac electromagnetic waves and thermal gradients [26–28]. The droplet is non-topological with a skyrmion number of zero; the skyrmion is topologically protected and has a skyrmion number of 1.

Despite these seemingly mutually exclusive properties, we here demonstrate how several of these characteristics can be successfully combined, yielding at the same time a dynamical and topologically protected magnetic soliton - a so-called dynamical skyrmion (DS). We develop an analytical theory to demonstrate that the DS is a generic solution, and its sustenance does not depend on DMI, DDI, and current-associated Oersted field. In the presence of DMI, however, the DS shows great potential for both strong microwave signal generation and novel skyrmionic functionality.

DYNAMICAL SKYRMIONS AS A GENERIC SOLUTION

As our starting point, we micromagnetically [29] model a NC-STO in zero applied field with an ultra-thin Co layer with strong PMA, without any DMI, and neglecting dipole-dipole interactions (DDI) (for the micromagnetic details, see Methods). As expected, we nucleate an ordinary magnetic droplet above a critical current given by the Slonczewski instability to auto-oscillations [17]. The droplet is characterized by a reversed core, with all spins precessing in phase, and a trivially zero skyrmion number $\mathcal{S} = \frac{1}{4\pi}\int\int n\,dx\,dy$ ($n = \mathbf{m}\cdot(\partial_x\mathbf{m}\times\partial_y\mathbf{m})$ being the topological density [30, 31] and $\mathbf{m}$ the magnetization unit vector).

However, if we increase the current density we find that there exists a second, higher, threshold current above which we, instead of a droplet, excite a precessing object with a *non-zero* skyrmion number. Fig. 1 presents the simulation results where panel Fig. 1a displays snap shots of the top view of the free layer magnetization, Fig. 1b the corresponding topological density, and Fig. 1c the time trace of the average out-of-plane magnetization component m_z and the corresponding skyrmion number (see also Supplementary Movie S1). After an initial relaxation, a current density of $J = 6\times10^8$ A/cm^2 is switched on. The system first forms a doughnut structure ($t_2 = 1.13$ ns and $t_3 = 1.15$ ns) due to the Oersted (Oe) field and eventually ($t_4 = 1.17$ ns) forms a dynamically precessing object, characterized by a fully reversed core, spins precessing along its perimeter, and $\mathcal{S} = 1$. This new state retains the dynamical precessing character of the droplet, while having the topology of a skyrmion, and can hence be described as a *dynamical skyrmion* (DS). Contrary to the droplet, where all spins precess in phase, the spins along the perimeter of the DS undergo a 2π rotation, leading to continuous transformations between hedgehog and vortex-like spin textures [32]. The spatially averaged in-plane magnetisation is hence constant in time. However, because of the large static Oe field, the DS experiences a time-varying Zeeman energy and as a consequence exhibits breathing at exactly the precession frequency; if we artificially turn off the Oe field ($t = 3$ ns) the breathing disappears. The breathing causes a strong variation in m_z that allows us to unambiguously determine the precession frequency. This behaviour is reminiscent of the breathing observed in quasi-1D magnetic droplet soliton pairs with non-zero chirality [33] and the DS indeed transforms into such a soliton pair if the lateral dimension of the simulation area is reduced to that of the NC (not shown).

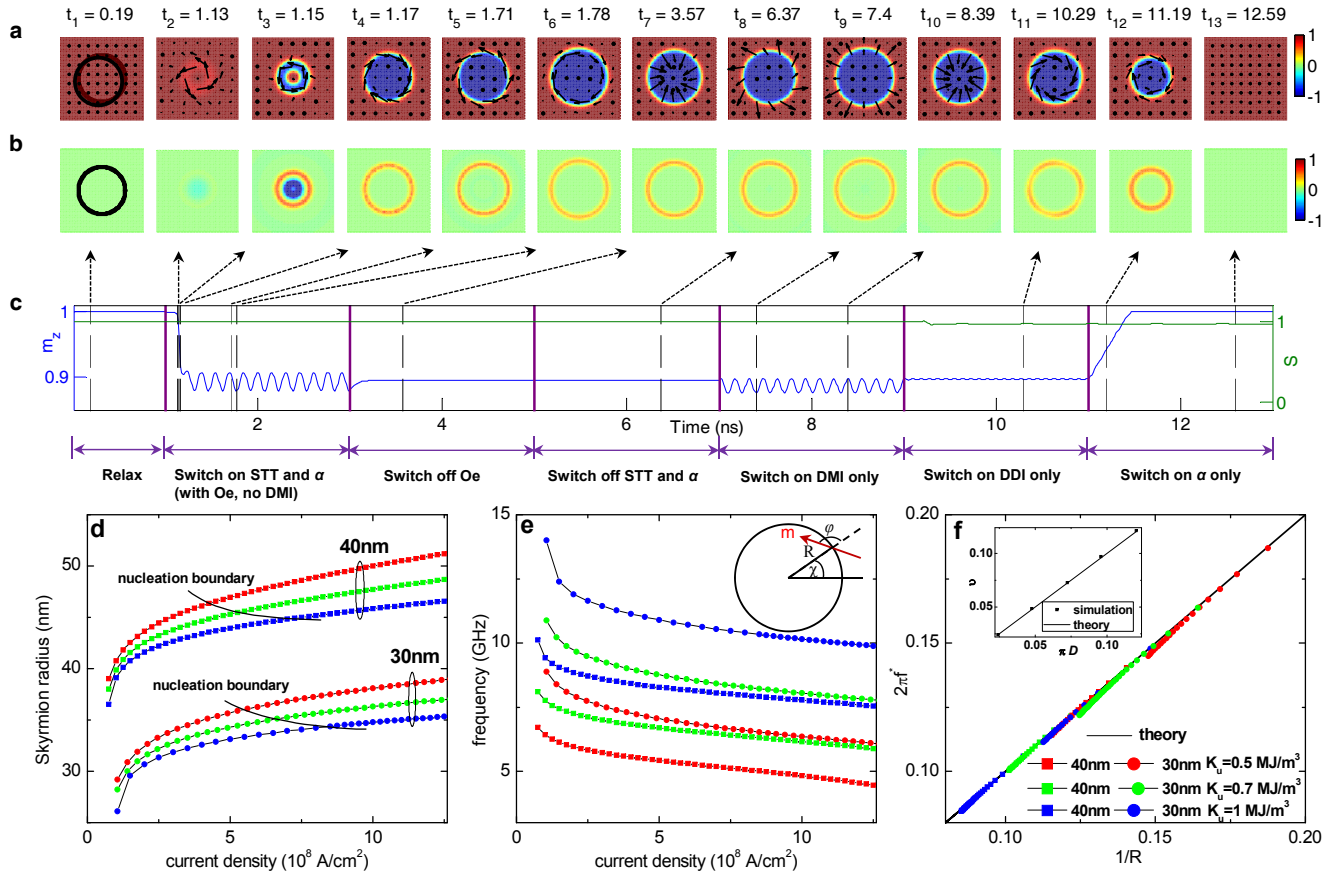

FIG. 1. **Nucleation and tuning of a dynamical skyrmion.** A micromagnetic simulation of a NC-STO with radius 40 nm and at $J = 6 \times 10^8$ A/cm^2 showing the nucleation of a dynamical skyrmion (DS) without DMI and DDI from an initial FM state and the subsequent tuning of the DS by STT, α, DMI, and DDI. **a** top-view of the spin structure at thirteen different times of the simulation; the black circle indicates the NC; **b** top-view of the topological density at the same times as in **a**; **c** time-trace of the out-of-plane m_z component averaged over the simulation area and time-trace of the skyrmion number; dashed vertical lines correspond to the thirteen snapshots above; **d** shows the DS radius vs current density for two NC sizes and three different PMA strengths; **e** shows the corresponding DS frequency; Inset shows the coordinate used in the theory. **f** shows the linear scaling law between the DS frequency and inverse radius, for currents at threshold and below, in excellent agreement with the analytical prediction. The inset shows the DMI-induced breathing amplitude $\nu = (R_{\max} - R_{\min})/(R_{\max} + R_{\min})$ as a function of D_0, in which the simulation results are again in excellent agreement with the theory. For panels **d-f**, $\alpha = 0.3$, D=0, with Oersted field.

If we simultaneously turn off both the current and the damping ($t = 5$ ns) the DS remains stable over time, indicating that it is a novel generic conservative soliton solution for a DMI-free PMA film in zero field. This is hence the topologically nontrivial counterpart of the well known non-topological magnon drop described in the 1970s [19, 20]. If we add a moderate DMI of 0.2 mJ/m^2 ($t = 7$ ns) m_z again varies in time and breathing resumes. If instead of DMI and Oe field we only turn on DDI ($t = 9$ ns), minor breathing is again observed, but this time at twice the precession frequency [20]. Finally, if only damping is turned on ($t = 11$ ns), the DS transforms into a uniform ferromagnetic state, accompanied with an emission of spin waves as shown in the Supplementary Movie S1. This again clearly demonstrates that the DS is not an excited state or an eigenmode of a static skyrmion, but a fundamentally novel solution in the form of a precessing skyrmion *without* the necessity of DMI or DDI.

As seen in Fig. 1d-e the NC size and the strength of the PMA (K_u) controls the overall frequency and radius of the DS, which can then be further actively tuned by the drive current: higher current increases the DS radius and red shifts its frequency. Remarkably, it is also possible to reduce the drive current well below the nucleation current without losing the DS. Similar to the droplet, the sustaining current of the DS can hence be much smaller than its nucleation current, resulting in a very large hysteresis in current.

These numerical results can be understood in terms of an effective analytical model. The cylindrical symmetry of

the DS lends itself to a description with the skyrmion radius $R(t)$ and the relative azimuthal angle $\varphi(t)$ as dynamical variables (for details see inset of Fig. 1e). As described in Supplementary Section S1, the Landau-Lifshitz-Gilbert-Slonczewski equation leads to the following effective equations of motion,

$$\dot{R} = F(\varphi, R) - \alpha\dot{\varphi} + \tilde{\sigma}(I)\tilde{\Theta}(a_c - R), \tag{1a}$$

$$\dot{\varphi} = \frac{1}{R} + \alpha\dot{R} \tag{1b}$$

The dot indicates a derivative with respect to time which is measured in units of the inverse anisotropy frequency $M_s/2\gamma K_u$. The skyrmion radius R is defined as the radius of the circle where $m_z = 0$ and is measured in units of the domain wall width $\delta_0 = \sqrt{A/K_u}$. $F(\varphi, R)$ is a function containing contributions from DMI, Oe-fields, and DDI, α is the damping constant, $\tilde{\sigma}(I)$ denotes the dimensionless spin-torque amplitude, and $\tilde{\Theta}(x)$ denotes the Heaviside step function smoothed over a length δ_0, and a_c is the radius of the NC measured in units of δ_0 (for details see Supplementary Section S1). Equation (1) holds under the assumption that $R > 1$.

The first order differential equations (1) capture the essence of the skyrmion dynamics observed in numerical simulations shown in Fig. 1. In the idealized case of an undamped and undriven system, $\alpha = \tilde{\sigma} = 0$, the instantaneous skyrmion radius and precession frequency obey the simple relation,

$$2\pi f^* R = 1, \tag{2}$$

where $f^* = \dot{\varphi}/2\pi$ is measured in units of the anisotropy frequency. As illustrated in Fig. 1f, our micromagnetic simulations follow this relation very closely without any adjustable parameters and even in presence of nonvanishing currents and finite damping, if the time average is taken over one period. Considering the fact that we map a micromagnetic system with many degrees of freedom onto an effective system with only two dynamical variables, such quantitative agreement is quite remarkable.

In the absence of DMI, Oe-fields, and DDI, m_z is conserved, and $F = 0$. In this case, both R and $\dot{\varphi}$ are constant in time, and a skyrmion with constant radius is stabilized by nonlinear uniform precession around the easy-axis, which satisfies $\mathcal{S} = 1$ at all times. It is remarkable that such a precessional DS can exist even in the absence of DMI, which is also observed in the full micromagnetic simulations (*cf.* Fig. 1a-c in the interval $5\,\text{ns} \leq t < 7\,\text{ns}$). Such behaviour persists in the presence of damping and compensating spin torque as is seen from the interval $3\,\text{ns} \leq t < 5\,\text{ns}$. In this case, equation (1) can be reduced to $(1+\alpha^2)\dot{R} = -\alpha/R + \tilde{\sigma}\tilde{\Theta}$ with solutions asymptotically converging to a time independent radius $R \approx \tilde{a}_c + \delta_0$. For $\tilde{\sigma} = 0$, the dynamics yields an ever shrinking skyrmion which eventually disappears due to lattice discreteness effects. This latter effect is seen in the simulations after $t = 11$ ns.

If in turn one of these interactions is nonzero, then $F \neq 0$, m_z is no longer conserved, and the time dependence of the precession frequency is obtained from $\ddot{\varphi} + F(\varphi)\dot{\varphi}^2 = 0$ (Supplementary Section S1). In the case of vanishing Oe-fields, this is R-independent and can readily be integrated. The solutions exhibit nonuniform precession and by virtue of equation (2), breathing of the skyrmion. Such breathing is indeed seen in the interval $7\,\text{ns} \leq t < 11\,\text{ns}$ of Fig. 1a-c (also refer to Supplementary Section S1).

A breathing skyrmion oscillates between radii $R_{\max}$ and $R_{\min}$ with corresponding relative azimuthal angles $\varphi_{\max}$ and $\varphi_{\min}$, respectively, which are in turn determined by the zeroes of $F(\varphi)$. If only DMI contributes then the reversal occurs at $\varphi_{\max} = 0$ and $\varphi_{\min} = \pi$ (t_9, t_{10} in Fig. 1). Thus at the largest extension, the skyrmion is in a hedgehog configuration favoured by DMI. For Oe-field $h_{\text{Oe}} < 0$ (*i.e.* current flowing downwards as in the simulations) we have $\varphi_{\max} = \pi/2$ and $\varphi_{\min} = 3\pi/2$, and thus at the largest radius, the skyrmion is in the energetically favoured tangential configuration oriented in a right handed fashion around the current (t_5, t_6 in Fig. 1). In these cases, breathing and precession frequency coincide. Finally, if only DDI contributes, then both time reversal and parity are unbroken and a skyrmion with maximal radius occurs at two values $\varphi_{\max} = \pi/2, 3\pi/2$, while $\varphi_{\min} = 0, \pi$. As a consequence, the radial oscillation frequency is twice the azimuthal frequency, which is indeed observed in the simulations in the interval $9\,\text{ns} < t \leq 11\,\text{ns}$.

In the case of DMI only, we also can easily compute the breathing amplitude ν upon time integration of equation (1a) over a half period. This yields $\nu = (R_{\max} - R_{\min})/(R_{\max} + R_{\min}) = \pi D_0$ with $D_0 = D/\mathcal{E}_0$ with $\mathcal{E}_0$ the domain wall energy per unit area. This relation is followed strikingly well in the presence of both current and damping as shown in the inset of Fig. 1f.

Interestingly, the critical current density for DS nucleation can be reduced dramatically (more than one order of magnitude) by using a smaller damping α, smaller K_u, and larger NC size (See Supplementary Section S2). Under these conditions, it becomes possible to create DS with relatively small current density in experiments. Furthermore, we confirmed that the above results and conclusions using a damping of α=0.3 remain qualitatively the same if a much smaller damping of α=0.05 is used (see Supplementary Section S2).

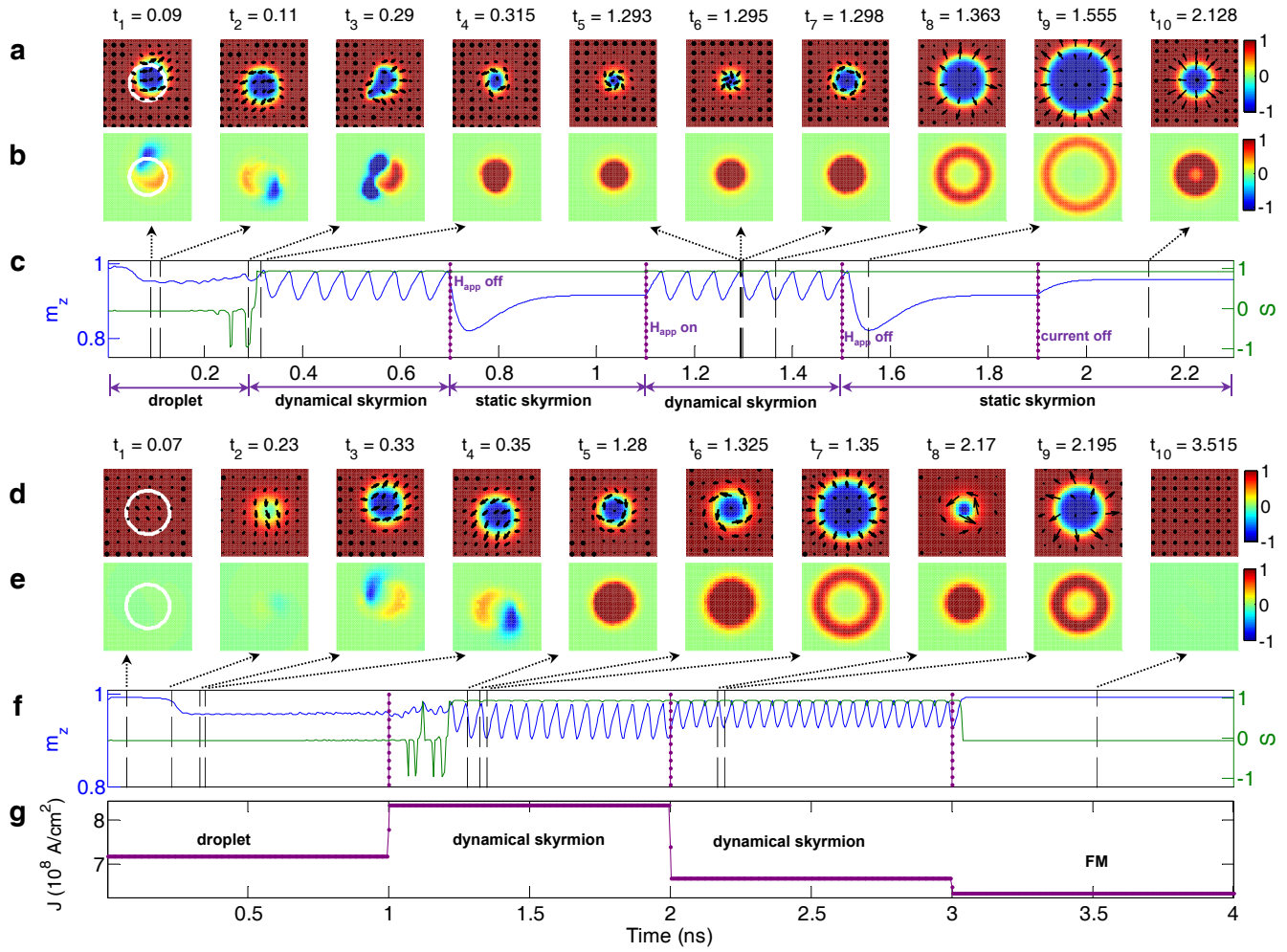

FIG. 2. **Nucleation, field- and current-toggling of a DS in presence of DMI.** Panels **a-c** show, respectively: the top-view of the spin structure at selected simulation times where the white circle indicates the 15nm NC; the topological density at the same times where the color-scale is normalized; the time-trace of the out-of-plane magnetization component m_z averaged over the simulation area; and time-trace of the skyrmion number (green). Panels **a-c** show droplet nucleation at $J = 8.3\times10^8$ A/cm^2 and $\mu_0 H_a = 0.3$ T, which remains stable for several periods until about $t = 0.2$ ns when it becomes increasingly susceptible to anti-skyrmion perturbation ($\mathcal{S} < 0$). These perturbations eventually ($t = 0.3$ ns) give way to the formation of a DS with $\mathcal{S} = 1$. When the applied field is turned off at $t = 0.7$ ns, the DS rapidly dissipatively shrinks into a static skyrmion. If the field is again turned on, the skyrmion can be transformed into a DS in a reversible manner. Finally, if both the field and the current are turned off, the static skyrmion contracts to its equilibrium size given by the material parameters. Panels **d-f** show a similar DS nucleation as a function of current and fixed field. The current density is varied as follows: $J = 7.2\times10^8$ A/cm^2 for 0 < t < 1 ns, 8.3×10^8 A/cm^2 for 1 ns < t < 2 ns , 6.7×10^8 A/cm^2 for 2 ns < t < 3 ns, and 6.3×10^8 A/cm^2 for 3 ns < t < 4 ns. Panel **g** schematically shows the current pulses applied during the simulation. See Supplementary Movie S2 and S3 for the entire process.

DYNAMICAL SKYRMIONS IN THE PRESENCE OF LARGE DMI

We now turn to the interesting case when the DS is nucleated and sustained in a material with large DMI. This situation is of particular applied importance as such systems are known to support static skyrmions and should hence allow for the interaction of droplets, skyrmions, and dynamical skyrmions. Figure 2a-d shows the rapid nucleation of a magnetic droplet soliton exhibiting its typical characteristics of precessing spins along its perimeter. Because of the large DMI, the spin structure is substantially perturbed (t_1 and t_2) compared to the situation where DMI is absent. At times t_1 and t_2, regions of weak non-zero topological density are found to rotate around the droplet perimeter. While the droplet is stable for a number of periods the topological perturbations continue to grow in amplitude and almost drive the formation of an anti-skyrmion ($\mathcal{S} \to -1$ at t_3) just before the system switches into a stable $\mathcal{S} = 1$

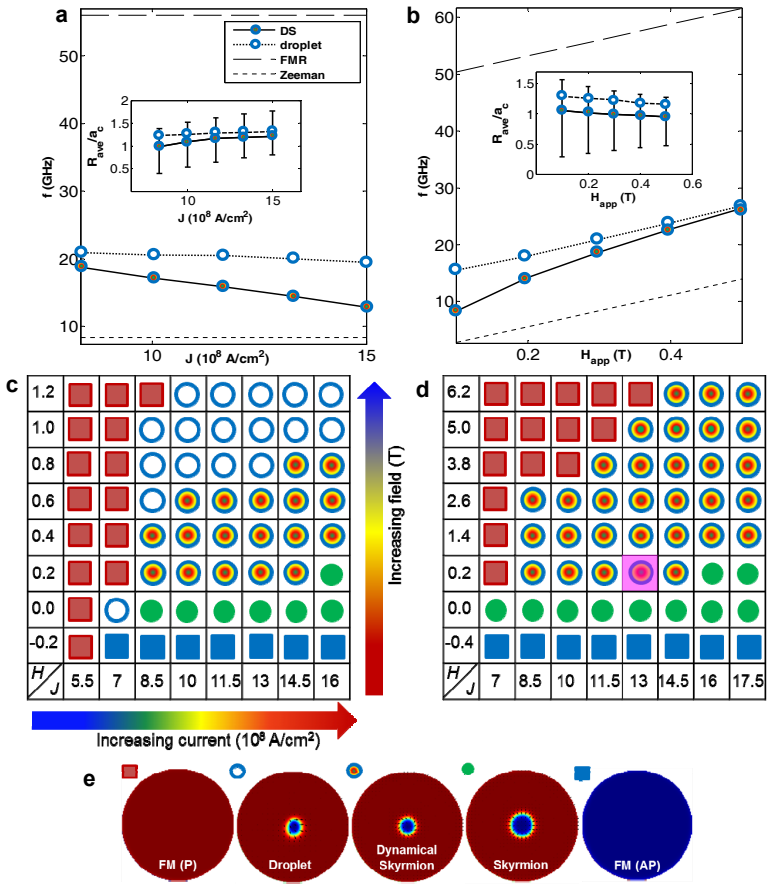

FIG. 3. **Frequency and stability of DS.** The frequency of the dynamical skyrmion is shown as solid lines and filled circles for: **a** $\mu_0 H_a = 0.3$ T while the current density is varied; **b** $J = 8.3 \times 10^8$ A/cm^2 while the applied field is varied. The corresponding droplet frequency (DMI=0) is shown as dotted lines and hollow circles. The Zeeman and FMR frequencies are shown as dashed lines. The insets show the radius of the droplet (hollow circles) and the time averaged radius of the dynamical skyrmion (filled circles) measured in units of NC radius where the error bars indicate the total range of radii values. The DS frequency decreases rapidly with increasing radius (increasing current) in **a**. As the field increases in **b**, the dynamical skyrmion becomes stiffer, reducing the breathing and making the dynamics resemble that of the droplet. **c** Nucleation of a droplet (hollow circle), dynamical skyrmion (filled rainbow circle), and static skyrmion (green filled circle) at different fields and currents. **d** Stability of the dynamical skyrmion over a very wide range of current and field. Note that the field axis is nonlinear to reach the final collapse of the dynamical skyrmion at very high fields. The DS was nucleated using the conditions highlighted by the pink square.

state at t_4. The transition mechanism occurs through a Bloch point pair or a single Bloch point on the surface (See Supplementary Section S3 for details).

If the applied field along $+z$ is turned off, the DS relaxes into a static hedgehog skyrmion; if the applied field is again turned on, the DS reforms as the precession restarts. The DS to static skyrmion transition is hence entirely reversible, which is a natural consequence of their identical topology. Finally, if both field and current are turned off, a smaller static hedgehog skyrmion remains with its size given by the DMI and material parameters of the simulation. From the STT provided by a non-zero current density, one can controllably tune the size of the static skyrmion, where a positive current density increases its size and a negative current density decreases it.

The DS can also be nucleated by controlling only the drive current density. Figure 2e-i shows a micromagnetic simulation of the same NC-STO in a constant applied field of 0.3 Tesla, which favours a uniform ferromagnetic state. After a period of weak FMR-like precession, a DMI-perturbed droplet forms and now remains stable for as long as the current density is limited to $J = 7.2 \times 10^8$ A/cm^2. When the current density is increased to $J = 8.3 \times 10^8$ A/cm^2 the

STT provides enough energy to induce strong topological fluctuations between negative and positive skyrmion numbers to finally switch the system into a stable dynamical skyrmion state. Once the dynamical skyrmion has formed, the current density can be reduced substantially while still sustaining the precession, until a minimum sustaining current density is reached below which the dynamical skyrmion rapidly collapses into a uniform $\mathcal{S} = 0$ ferromagnetic state, in a similar fashion as ordinary droplets. As a consequence it is perfectly possible to repeatedly access the uniform, droplet, and dynamical skyrmion states by only controlling the current density. By controlling *both* the drive current density and the applied field, transitions between all four states, including the static skyrmion, can be controlled at will, with the only limitation being the direct transformation of a skyrmion or dynamical skyrmion into a droplet, which requires an intermediate step of a uniformly magnetized state.

In Fig. 3a-b we compare the field- and current-dependent tunability of the DS and the corresponding droplet (the latter simulated by removing the DMI term but otherwise sharing identical conditions). The most salient feature of the DS is a much stronger frequency tunability than the droplet. Whereas the droplet frequency is essentially independent of current density and linearly dependent on the field, the frequency of the DS decreases rapidly and linearly with increasing current density and exhibits a non-linear field dependence, in particular at low fields. Additionally, the DS maximum frequency is bounded by its droplet counterpart.

The key to understanding the much stronger field- and current dependencies lies in the very strong breathing of the DS, which dominates the dynamics at large DMI. While the ordinary droplet is always slightly larger than the NC, and does not vary in size significantly with either current or field, the radius of the dynamical skyrmion can at low fields have a minimum that is less than a third of the NC radius and a maximum that is more than 50% greater than the NC, as shown by the error bars in the insets in Fig. 3. In other words, the breathing can make the dynamical skyrmion radius vary by more than five times of its minimum size. The very strong breathing will increase the dissipation and the periodic translation of the domain wall making up the dynamical skyrmion perimeter will slow down the overall precession. When the current density is increased in Fig. 3a the maximum radius also increases, further slowing down the precession. However, when the field is increased in Fig. 3b the dynamical skyrmion stiffens, the amplitude of the breathing decreases, and as a consequence, both the the maximum radius and the frequency of the dynamical skyrmion approach those of the droplet.

As observed in Fig. 2 above, the DS exhibits a similar degree of hysteresis as the original droplet, *i.e.* its sustaining current can be much lower than the current needed for nucleation. This hysteresis ensures a minimum degree of stability, which should make the DS sufficiently robust for applications. In Fig. 3, we investigate this stability in more detail and present a nucleation phase diagram in Fig. 3c and a stability phase diagram in Fig. 3d. The nucleation phase diagram presents the final steady state of the simulated system, when both current and field are turned on at t_0 and held constant until steady state. Five different end states can be identified: a droplet, a DS, a static skyrmion, and the two trivially saturated states. The stability phase diagram, on the other hand, presents the final steady state at all field and current values after a DS has first been nucleated at the conditions shown in pink. Here, only four different end states are possible as the DS never transforms back directly into a droplet. It is noteworthy that the DS is stable over a very large current and field range, more so than the droplet, which is consistent with its topological protection affording it additional stability.

In summary, we have demonstrated how droplets and skyrmions can be combined to form a dynamical skyrmion, a hitherto unknown topological and dissipative magnetic soliton with great potential for both new physics and direct applications in skyrmionics and NC- based microwave signal generators.

METHODS

Micromagnetic simulations

Micromagnetic simulations are performed for the free layer with the graphics-processing-unit-based tool Mumax3 [29]. The time-dependent spin dynamics follow the Landau-Lifshitz-Gilbert-Slonczewski equation of motion,

$$\frac{d\mathbf{m}}{dt} = -|\gamma|\mathbf{m} \times \mu_0\mathbf{H}_{eff} + \alpha\mathbf{m} \times \frac{d\mathbf{m}}{dt} + |\gamma|\mu_0 M_s \sigma(I) f(\vec{r}) \epsilon \mathbf{m} \times (\mathbf{m} \times \hat{\mathbf{z}}), \tag{3}$$

where $|\gamma|/2\pi$=28 GHz/T is the gyromagnetic ratio, α is the Gilbert damping parameter, μ_0 is the magnetic vacuum permeability, M_s is the free layer saturation magnetisation, and $\mathbf{m}$ is the free layer normalized magnetisation vector. The fixed layer magnetisation vector is along $+\hat{\mathbf{z}}$. $\sigma(I) = \hbar IP\lambda/\mu_0 M_s^2 eV(\lambda+1)$ is the dimensionless spin torque coefficient where $\hbar$ is the reduced Planck constant, I is the electric current, P is spin polarization, e is the elementary

charge ($e > 0$), V is the free layer volume. $\epsilon^{-1} = 1 + \frac{\lambda - 1}{\lambda + 1}\hat{m} \cdot \hat{\mathbf{z}}$, where λ is the magnetoresistance (MR) asymmetry parameter describing the deviation from sinusoidal angular dependence. $f(\vec{r})$ is the Heaviside step function approximately describing the current distribution, *i.e.* $f(\vec{r})$=1 for $r \leq a_c\delta_0$ and 0 otherwise. The effective field $\vec{H}_{eff}$ includes the contribution from Heisenberg exchange, PMA, DMI, and an applied external field along the $+\hat{\mathbf{z}}$ direction. The DMI in Mumax3 is assumed to be purely of interfacial origin, giving rise to the energy [34].

$$\epsilon_{DM} = D\left(m_z\frac{\partial m_x}{\partial x} - m_x\frac{\partial m_z}{\partial x} + m_z\frac{\partial m_y}{\partial y} - m_y\frac{\partial m_z}{\partial y}\right) \tag{4}$$

where D is the DMI constant in units of J/m^2.

A NC spin torque oscillator geometry is modeled, based on a pseudo spin valve with PMA fixed and free layers and a current-confining NC of radius 15 nm placed at the centre of the free layer (except in Fig. 1 where the NC radius is varied between 30 nm and 40 nm). The free layer is assumed to be a 1 nm thick Co film with radius of 100 nm on a substrate inducing DMI, which can be controlled by varying the layer thickness, and material parameters similar to Ref. [13], namely: exchange constant $A = 15$ pJ/m, Gilbert damping $\alpha = 0.3$, spin polarization ratio P=0.3, saturation magnetisation $M_s = 580$kA/m, $D = 3$ mJ/m^2 and $K_u = 0.7$ MJ/m^3 unless otherwise specified. These parameters lead to a domain-wall width of $\delta_0 = 5.6$ nm. The fixed layer is assumed to be magnetised along the +z direction, inducing a STT with $\lambda = 1$ for simplicity. All of our simulations are performed with unit cell size between 1 and 2 nm, which is well below δ_0 and the exchange length, ensuring numerical accuracy. For finite temperature simulations in Supplementary Section S4, a fixed time step of 0.1 fs is used. The simulations are performed with open boundary conditions, *i.e.* damping is set to be uniform across the whole disk including the boundary (for details see Supplementary Section S5).

[1] Roessler, U. K., Bogdanov, A. N. & Pfleiderer, C. Spontaneous skyrmion ground states in magnetic metals. *Nature* **442**, 797–801 (2006).
[2] Heinze, S. *et al.* Spontaneous atomic-scale magnetic skyrmion lattice in two dimensions. *Nature Physics* **7**, 713–718 (2011).
[3] Schulz, T. *et al.* Emergent electrodynamics of skyrmions in a chiral magnet. *Nature Physics* **8**, 301–304 (2012).
[4] Seki, S., Yu, X. Z., Ishiwata, S. & Tokura, Y. Observation of skyrmions in a multiferroic material. *Science* **336**, 198–201 (2012).
[5] Nagao, M. *et al.* Direct observation and dynamics of spontaneous skyrmion-like magnetic domains in a ferromagnet. *Nature Nanotechnology* **8**, 325–328 (2013).
[6] Ritz, R. *et al.* Formation of a topological non-fermi liquid in MnSi. *Nature* **497**, 231–234 (2013).
[7] Milde, P. *et al.* Unwinding of a skyrmion lattice by magnetic monopoles. *Science* **340**, 1076–1080 (2013).
[8] Nagaosa, N. & Tokura, Y. Topological properties and dynamics of magnetic skyrmions. *Nature Nanotechnology* **8**, 899–911 (2013).
[9] Brataas, A. & Hals, K. M. D. Spin-orbit torques in action. *Nature Nanotechnology* **9**, 86–88 (2014).
[10] Mühlbauer, S. *et al.* Skyrmion lattice in a chiral magnet. *Science* **323**, 915–919 (2009).
[11] Yu, X. *et al.* Real-space observation of a two-dimensional skyrmion crystal. *Nature* **465**, 901 – 904 (2010).
[12] Yu, X. *et al.* Near room-temperature formation of a skyrmion crystal in thin-films of the helimagnet FeGe. *Nature Materials* **10**, 106 – 109 (2011).
[13] Sampaio, J., Cros, V., Rohart, S., Thiaville, A. & Fert, A. Nucleation, stability and current-induced motion of isolated magnetic skyrmions in nanostructures. *Nature Nanotechnology* **8**, 839–844 (2013).
[14] Fert, A., Cros, V. & Sampaio, J. Skyrmions on the track. *Nature Nanotechnology* **8**, 152 – 156 (2013).
[15] Iwasaki, J., Mochizuki, M. & Nagaosa, N. Current-induced skyrmion dynamics in constricted geometries. *Nature Nanotechnol* **8**, 742 (2013).
[16] Romming, N. *et al.* Writing and deleting single magnetic skyrmions. *Science* **341**, 636–639 (2013).
[17] Hoefer, M. A., Silva, T. J. & Keller, M. W. Theory for a dissipative droplet soliton excited by a spin torque nanocontact. *Phys. Rev. B* **82**, 054432 (2010).
[18] Mohseni, S. M. *et al.* Spin torque generated magnetic droplet solitons. *Science* **339**, 1295–1298 (2013).
[19] Ivanov, B. & Kosevich, A. Bound states of a large number of magnons in a ferromagnet with a single-ion anisotropy. *Sov. Phys. JETP* **45**, 1050 (1977).
[20] Kosevich, A., Ivanov, B. & Kovalev, A. Magnetic solitons. *Physics Reports* **194**, 117 – 238 (1990).
[21] Slonczewski, J. C. Current-driven excitation of magnetic multilayers. *Journal of Magnetism and Magnetic Materials* **159**, L1 – L7 (1996).
[22] Berger, L. Emission of spin waves by a magnetic multilayer traversed by a current. *Phys. Rev. B* **54**, 9353–9358 (1996).
[23] Rippard, W. H. *et al.* Spin-transfer dynamics in spin valves with out-of-plane magnetized free layers. *Phys. Rev. B* **81**, 014426 (2010).

[24] Mohseni, S. M. *et al.* High frequency operation of a spin-torque oscillator at low field. *Physica Status Solidi RRL* **5**, 432 – 434 (2011).
[25] Hoefer, M. A., Sommacal, M. & Silva, T. J. Propagation and control of nanoscale magnetic-droplet solitons. *Phys. Rev. B* **85**, 214433 (2012).
[26] Mochizuki, M. Spin-wave modes and their intense excitation effects in skyrmion crystals. *Phys. Rev. Lett.* **108**, 017601 (2012).
[27] Onose, Y., Okamura, Y., Seki, S., Ishiwata, S. & Tokura, Y. Observation of magnetic excitations of skyrmion crystal in a helimagnetic insulator Cu_2OSeO_3. *Phys. Rev. Lett.* **109**, 037603 (2012).
[28] Mochizuki, M. *et al.* Thermally driven ratchet motion of a skyrmion microcrystal and topological magnon Hall effect. *Nature Materials* **13**, 241–246 (2014).
[29] Vansteenkiste, A. & de Wiele, B. V. Mumax: A new high-performance micromagnetic simulation tool. *Journal of Magnetism and Magnetic Materials* **323**, 2585 – 2591 (2011).
[30] Moutafis, C., Komineas, S. & Bland, J. A. C. Dynamics and switching processes for magnetic bubbles in nanoelements. *Phys. Rev. B* **79**, 224429 (2009).
[31] Braun, H. B. Topological effects in nanomagnetism: from superparamagnetism to chiral quantum solitons. *Advances in Physics* **61**, 1–116 (2012).
[32] Thiaville, A., Rohart, S., Jue, E., Cros, V. & Fert, A. Dynamics of dzyaloshinskii domain walls in ultrathin magnetic films. *EPL* **100**, 57002 (2012).
[33] Iacocca, E. *et al.* Confined dissipative droplet solitons in spin-valve nanowires with perpendicular magnetic anisotropy. *Phys. Rev. Lett.* **112**, 047201 (2014).
[34] Bogdanov, A. N. & Rößler, U. K. Chiral symmetry breaking in magnetic thin films and multilayers. *Phys. Rev. Lett.* **87**, 037203 (2001).

ACKNOWLEDGEMENTS

Y.Z. thanks the support by the UGC Grant AoE/P-04/08 of Hong Kong SAR government. H.B.B. acknowledges financial support from Science Foundation Ireland (Grant No. 11/PI/1048). This work was partially supported by the ERC Starting Grant 307144 "MUSTANG", the Swedish Foundation for Strategic Research (SSF) program Future Research Leaders, the Swedish Research Council (VR), and the Knut and Alice Wallenberg Foundation. Johan Åkerman is a Royal Swedish Academy of Sciences Research Fellow supported by a grant from the Knut and Alice Wallenberg Foundation.